

Current Biology, Volume 24

Supplemental Information

**Retrograde Plasticity and Differential
Competition of Bipolar Cell Dendrites
and Axons in the Developing Retina**

Robert E. Johnson and Daniel Kerschensteiner

Figure S1

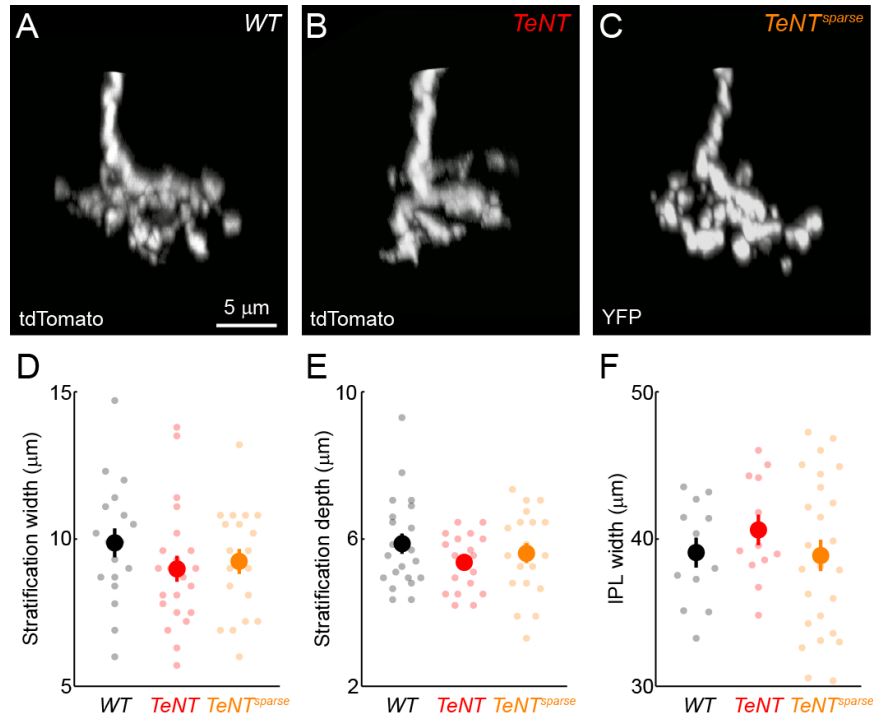


Figure S1. Silenced axons stratify normally.

(A-C) Orthogonal maximum intensity projections of confocal image stacks of representative B6 axons acquired in flat-mounted *WT* (A), *TeNT* (B) and *TeNT^{sparse}* (C) retinas.

(D) Comparison of distances along the z-axis from deepest to shallowest branch of B6 axons (i.e. stratification width) between *WT* (n = 18), *TeNT* (n = 22) and *TeNT^{sparse}* (n = 19) mice (p > 0.19 for all comparisons).

(E) Quantification of the midpoints of B6 axon arbors from the border between the ganglion cell layer and the IPL (i.e. stratification depth) in *WT* (n = 21), *TeNT* (n = 18) and *TeNT^{sparse}* (n = 19) mice (p > 0.15 for all comparisons).

(F) Total IPL widths measured in vibratome slices stained for VAMP2 between *WT* (n = 12), *TeNT* (n = 12) and *TeNT^{sparse}* (n = 25) mice (p > 0.3 for all comparisons).

In (D-F) each small circle represents one cell (D, E) or one retinal slice (F) and large filled circles (errorbars) indicate the population averages (\pm SEM).

Related to Figure 2.

Figure S2

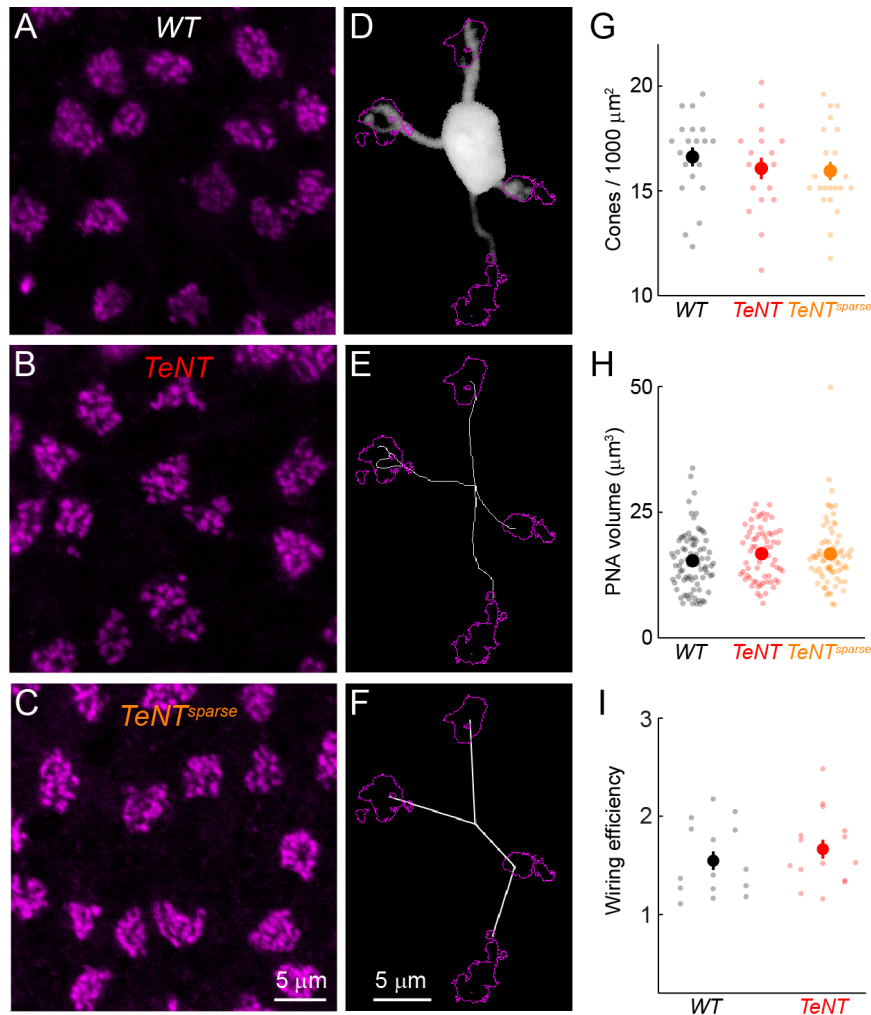


Figure S2. Numbers and sizes of cone terminals are conserved among *WT*, *TeNT* and *TeNT^{sparse}* retinas and wiring efficiency of B6 dendrites is unchanged in *TeNT* retinas.

(A-C) Representative confocal images of cone terminals labeled with fluorescent PNA in the OPLs of *WT* (A), *TeNT* (B) and *TeNT^{sparse}* (C) retinas.

Because the number of cones contacted by B6 dendrites in *TeNT* mice was unchanged compared to *WT* littermates (Figure 3), we wanted to explore more subtle changes of dendritic arborization in *TeNT* retinas.

(D) Maximum intensity projection through a confocal images stack of a representative B6 dendritic tree in a *WT* retina. Positions and shapes of cone active zones contacted by the B6 are outlined in *magenta*.

(E) Shows the dendritic skeleton determined using the Simple Neurite Tracer plugin in ImageJ (NIH).

(F) Illustrates the minimal spanning tree calculated using Prim's algorithm in Matlab. In (E) and (F) the x/y -centers of mass of synaptic contacts and the soma were set as obligatory nodes of the respective graphs.

(G) Quantification of the density of cone terminals in *WT* ($n = 20$), *TeNT* ($n = 18$) and *TeNT^{sparse}* ($n = 21$) mice ($p > 0.29$ for all comparisons).

(H) Active zone volumes of cones measured by local threshold masks of fluorescent PNA signals in *WT* ($n = 80$), *TeNT* ($n = 67$) and *TeNT^{sparse}* ($n = 71$) mice ($p > 0.13$ for all comparisons).

(I) Comparison of the wiring efficiency (i.e. ratio of the length of the dendritic skeleton over the length of the minimal spanning tree) between B6 dendrites in *WT* ($n = 15$) and *TeNT* ($n = 15$) retinas ($p > 0.38$).

In (G - I) each small circle represents one retina (G), one cone (H), and one BC (I) respectively. Large filled circles (errorbars) indicate the population averages (\pm SEM).

Related to Figure 3.

Figure S3

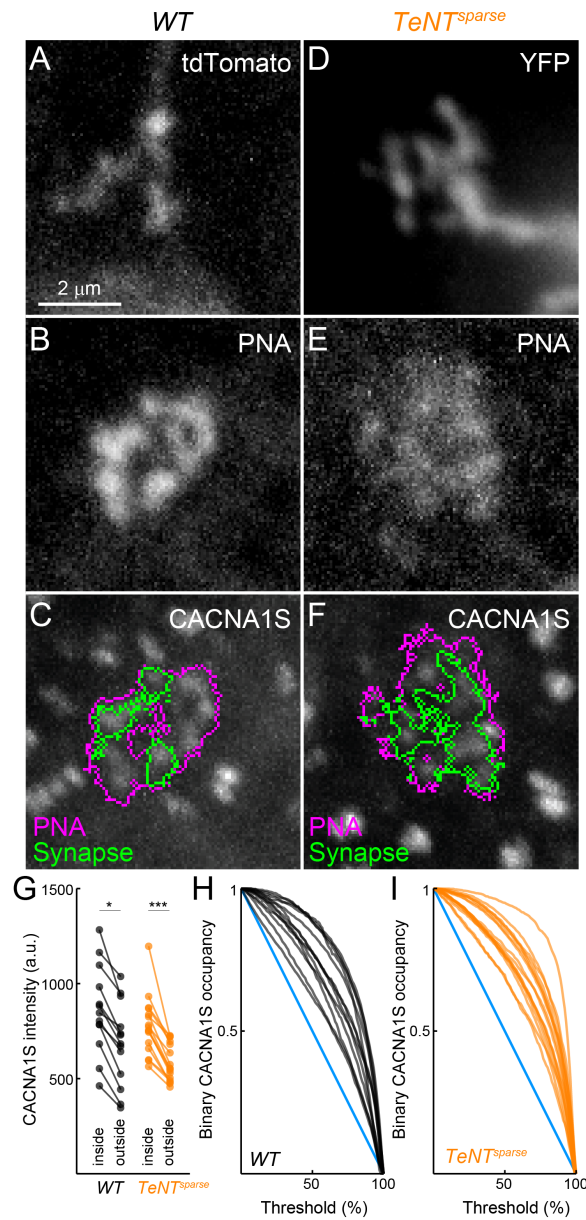


Figure S3. Synaptic contacts between cones and dendrites of silenced B6s in *TeNT^{sparse}* mice differentiate normally.

The size of contacts between B6 dendrites and cones was drastically increased in *TeNT^{sparse}* compared to *WT* littermates. We therefore wanted to test whether synaptic specialization of enlarged contacts was preserved.

(A-F) Representative confocal images of contacts between bipolar cell dendrites visualized by transgenic expression of fluorescent proteins (A, D) and cone active zones stained with fluorescent PNA (B, E) in *WT* (A, B) and *TeNT^{sparse}* (D, E) retinas. Labeling for CACNA1S, which localizes selectively to postsynaptic specializations of ON BCs [S1] in both genotypes is shown in (C, *WT*) and (F, *TeNT^{sparse}*). Cone active zones and areas of overlap with the dendrite of a B6 are outlined in *magenta* and *green*, respectively, in both panels.

(G) Comparison of the mean intensity of CACNA1S staining within (*inside*) synaptic contacts with labeled B6s and *outside* a binary mask of the PNA signal (*WT*: $n = 13$, $p < 0.05$, *TeNT^{sparse}*: $n = 15$, $p < 0.001$). In this analysis a 3-dimensional region centered on each cone pedicle of interest was cropped and the voxels occupied by the cone pedicle identified based on local thresholding of the PNA signal. The B6 dendrite contacting this cone pedicle was also masked. The overlap of these two masks identifies the voxels that are *inside* the synapse between this B6 dendrite and the cone pedicle. The CACNA1S intensity values in these voxels were compared to the CACNA1S intensity values of all voxels excluded from the PNA binary mask (i.e. *outside*). Note that *outside* parts of the image include synaptic contacts between rods and their postsynaptic partners.

(H, I) Line plots showing the decrease in territory occupancy of synaptic contacts by CACNA1S staining as a function of increasing thresholds of the CACNA1S signal in *WT* (C) and *TeNT^{sparse}* (F) retinas.

Related to Figure 3.

Figure S4

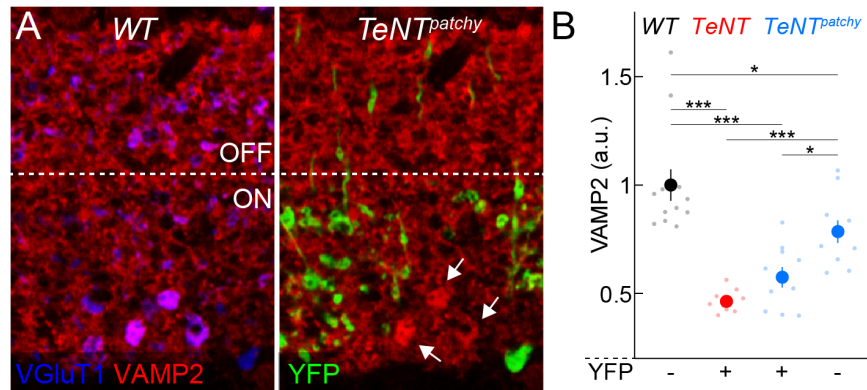


Figure S4. The pattern of VAMP2 depletion matches that of YFP expression in *TeNT^{patchy}* mice. (A) Representative image of the IPL of a *TeNT^{patchy}* retina showing that VAMP2 is depleted in axon terminals (VGLUT1) of TeNT-expressing (i.e. YFP-positive) ON BCs to a greater extent than in YFP-negative terminals of ON BCs. (B) Quantification of the VAMP2 content of YFP-negative (*WT*: n = 12, *TeNT^{patchy}*: n = 10) and YFP-positive (*TeNT*: n = 10, *TeNT^{patchy}*) ON BC axon terminals. Each small circle represents one retina and large filled circles (errorbars) indicate the population averages (\pm SEM).

Related to Figure 4.

Supplemental Experimental Procedures

Mice. To suppress transmitter release from B6 axons *in vivo*, we used mice in which a 9 kb fragment of the *Grm6* promoter [S2] drives expression of the light chain of tetanus toxin (TeNT) and yellow fluorescent protein (YFP). We previously characterized transgenic lines with nearly uniform expression among ON BCs, including B6 (*TeNT* mice) [S3, 4]. For the present study, we generated additional mice using the same construct in which, likely due to position effect variegation, expression was restricted to a sparse subset of B6s (*TeNT^{sparse}* mice). In addition, we identified founders in which the density of TeNT expression varied in patches across the retinal surface (*TeNT^{patchy}* mice). To visualize individual B6s in control (*WT*), *TeNT* and *TeNT^{patchy}* mice, these lines were crossed to *tdTomato* mice, in which few B6 cells per retina exhibit bright red fluorescence [S3]. Silenced B6s in *TeNT^{sparse}* mice were reconstructed based on their YFP signal.

Tissue preparation. All procedures were approved by the Animal Studies Committee of Washington University School of Medicine and complied with the National Institutes of Health *Guide for the Care and Use of Laboratory Animals*. Mice were deeply anesthetized with CO₂, killed by cervical dislocation and their eyes removed. Retinas were isolated and mounted in agarose or flattened on membrane discs. For multielectrode array (MEA) recordings, mice were dark adapted for approximately 2 h prior to enucleation and retinas prepared under infrared (>900 nm) illumination. For immunohistochemistry, tissue was fixed for 30 min in 4% paraformaldehyde in mouse artificial cerebrospinal fluid (mACSF), washed for > 10 min in PBS, washed in 10% sucrose in PBS for 1 h at RT, washed in 20% sucrose in PBS for 1 h at RT, washed in 30% sucrose in PBS overnight at 4° C, freeze-thawed 3 times, washed in PBS for > 10 min and incubated in 5% normal donkey serum for 2 h prior to addition of primary antibodies.

Immunohistochemistry. Vibratome sections (60 μm) and retinal flat mounts were incubated with mouse anti-CACNA1S (1:500, Millipore), mouse anti-CtBP2 (1:500, BD Bioscience), rabbit anti-GFP (1:1000, Millipore), mouse anti-VAMP2 (1:500, Synaptic Systems) or guinea pig anti-VGluT1 (1:1000, Millipore) for one (vibratome slices) or five days (flat mounts) at 4° C. The tissue was then washed in PBS (3 x 30 min), incubated with DyLight 405- (1:100, Jackson ImmunoResearch), Alexa Fluor 488-, Alexa Fluor 568- and/or Alexa Fluor 633-conjugated secondary antibodies (1:1000, Invitrogen) for 2 h at RT (vibratome slices) or two days at 4° C (flat mounts), washed again in PBS (3 x 30 min) and mounted in Vectashield mounting medium

(Vector Laboratories) for confocal imaging. PNA conjugated to Alexa Fluor 488, Alexa Fluor 568, or Alexa Fluor 647 (1:200, Invitrogen) was added with secondary antibodies.

Imaging and analysis. Image stacks were acquired on an Fv1000 confocal laser scanning microscope (Olympus) using a 60X 1.35 NA oil-immersion objective. Voxel sizes ($x/y - z$) were 0.066-0.3 μm for B6 axonal and dendritic synapse analyses and 0.069-0.3 μm for somatic images and VAMP2 analysis. For VAMP2 quantification, identically sized rectangular regions of the ON and OFF sublaminae were analyzed in single image planes of IPL. For *WT* retinas, the VGlut1 channel of the ON sublamina image was thresholded (top 20% brightest pixels) to identify ON BC terminals in the VAMP2 channel. The same procedure was used to isolate BC terminals in the OFF sublamina in all experiments. The average VAMP2 intensity in ON BCs of a given section was divided by the average VAMP2 intensity in OFF BCs of the same section and the mean ON/OFF BC VAMP2 ratio in *WT* retinas used to normalize measurements across genotypes. For ON BCs in *TeNT*, *TeNT^{sparse}* and *TeNT^{patchy}* mice, VAMP2 content was analyzed separately for YFP-positive (i.e. *TeNT* expressing) and YFP-negative axon terminals based on masks generated by local thresholding in Amira (FEI Company).

To analyze output connectivity of B6s, axons of individual neurons were masked in 3D using local thresholding in Amira (FEI Company). Axon masks were applied to their corresponding CtBP2 image stacks and synapse positions identified using custom written Matlab (The Mathworks) routines [S3, 4]. To analyze input connectivity of B6s, dendritic branches and active zones of cone pedicles labeled with fluorescent PNA were masked in 3D using local thresholding in Amira. Both 3D masks were multiplied to reveal regions of overlap and the resulting stack projected along its z -axis to give a 2D measurement of cone-B6 contact (i.e. synapse area). Due to the elongation of the point spread function in the z -dimension, some dendritic processes contacting cones directly above a cell body were contaminated by light emitted from the soma and could not be masked accurately. Contacts of these processes with cones were removed from synaptic area analyses. The distance from a cone contact to the soma center was calculated as the distance from the center of mass in the x/y plane of the synaptic overlap to the x/y position of the soma center.

To compare synaptic differentiation of cone-B6 contacts in *WT* and *TeNT^{sparse}* retinas, dendrites and cone active zones were masked as described above. Images of individual contacts were cropped to 6.66 x 6.66 μm in x/y and those z -planes that included overlap of the dendrite and cone pedicle. Signals of immunostaining for CACNA1S, a protein localized

specifically to postsynaptic densities of BC dendrites [S1], were iteratively thresholded and occupancy of the dendrite-cone contact volume calculated at each threshold.

Electroretinography and analysis. Electroretinograms (ERGs) were recorded and analyzed as as described previously [S5]. Briefly, ERG responses to brief white light flashes (< 5 ms) were acquired from *TeNT* mice and *WT* littermates (P30) using a UTAS Visual Electrodiagnostic Testing System (LKC Technologies). Mice dark adapted overnight were anaesthetized with ketamine (80 mg/kg) and xylazine (15 mg/kg) and their pupils dilated with 1% atropine sulfate (Falcon Pharmaceuticals). Recording electrodes embedded in contact lenses were placed over the cornea of each eye. At each light level 5-10 responses were averaged. The a-wave amplitude was reported as the difference between the response minimum in the first 50 ms after flash onset and the voltage value at flash onset. The b-wave amplitude was reported as the difference between a 15-25 Hz low-pass-filtered b-wave peak and the a-wave amplitude. The oscillatory potential amplitude was reported as the difference between the maximum and minimum values of the response after being filtered by a zero-phase 100 Hz high-pass filter. All ERG analyses were performed using custom scripts written in Matlab.

Multielectrode array recordings and analysis. Retinas were isolated in cold (4° C) carbogenated (95% O₂, 5% CO₂) mACSF containing (in mM): 125 NaCl, 2.5 KCl, 1.25 NaH₂PO₄, 2 CaCl₂, 1. MgCl₂, 20 Glucose, 26 NaHCO₃, 0.5 L-Glutamine. Isolated retinas were incubated in hyaluronidase (0.5 mg/mL in mACSF) at RT for 30 min, trimmed, placed GC side down on a 252 MEA (electrode diameter: 30 μm, electrode spacing: 100 μm) and covered with a transparent dialysis membrane (MWCO: 25 kDa, Spectrum Labs) held in place by a platinum ring. Preparations were allowed to settle in darkness (<0.01 Rh*/R/s) for 1 h. Throughout this period and the subsequent recording retinas were continuously superfused with warm (34° C) carbogenated mACSF.

Checkerboard Gaussian white noise was presented for 1 h from an organic light emitting display (xOLED, eMagin) focused on the photoreceptors through a 10X objective. The intensity of each stimulus square (28 μm x 28 μm on the retina) was chosen independently from a Gaussian distribution (mean: ~ 4000 Rh*/rod/s, contrast: 35 %) every 33 ms (refresh rate: 30 Hz). MEA signals were bandpass filtered (300 Hz – 3 kHz), digitized at 10 kHz and spike waveforms sorted into single units in Offline Sorter (Plexon). Only units with clean refractory periods and average firing rates > 0.55 Hz during white noise stimulation were analyzed further.

ON GC RFs were characterized by computing spike-triggered average (STA) stimuli (1 ms bins, duration: 500 ms prior to spiking) [S6, 7]. To identify significant ON pixels in each STA a threshold was determined as follows: STAs were simulated 10 times each for 10, 20, 50, 100, 500, 1000, 5000, and 10000 random events. The maximum pixel value in the 120 x 160 x 500 STA array of each simulation was recorded and the change in its average plus 2 SDs with increasing event count fit to a 2-term power function. Thus, the threshold for ON pixel significance decreased as a function of the number of spikes used to calculate the STA. The spatial structure of ON GC RFs was analyzed in the STA frame with the most significant pixels. RF maps with fewer than 3 significant pixels or extending beyond a 15 x 15 pixel region centered on the center of mass of the RF were excluded from the analysis. RF solidity was calculated as the ratio of the area of the sum of all significant pixels over the area of the smallest convex polygon to encompass them.

Statistics. Two-sided t-tests, with Bonferroni correction for multiple comparisons where appropriate, were used to test for significant differences between experimental groups. Unless noted otherwise, *, ** and *** indicate $p < 0.05$, 0.01 and 0.001, respectively.

Supplemental References

- S1. Specht, D., Wu, S.B., Turner, P., Dearden, P., Koentgen, F., Wolfrum, U., Maw, M., Brandstatter, J.H., and tom Dieck, S. (2009). Effects of presynaptic mutations on a postsynaptic Cacna1s calcium channel colocalized with mGluR6 at mouse photoreceptor ribbon synapses. *Investigative ophthalmology & visual science* 50, 505-515.
- S2. Ueda, Y., Iwakabe, H., Masu, M., Suzuki, M., and Nakanishi, S. (1997). The mGluR6 5' upstream transgene sequence directs a cell-specific and developmentally regulated expression in retinal rod and ON-type cone bipolar cells. *J Neurosci* 17, 3014-3023.
- S3. Kerschensteiner, D., Morgan, J.L., Parker, E.D., Lewis, R.M., and Wong, R.O. (2009). Neurotransmission selectively regulates synapse formation in parallel circuits in vivo. *Nature* 460, 1016-1020.
- S4. Morgan, J.L., Soto, F., Wong, R.O., and Kerschensteiner, D. (2011). Development of cell type-specific connectivity patterns of converging excitatory axons in the retina. *Neuron* 71, 1014-1021.
- S5. Soto, F., Watkins, K.L., Johnson, R.E., Schottler, F., and Kerschensteiner, D. (2013). NGL-2 regulates pathway-specific neurite growth and lamination, synapse formation, and signal transmission in the retina. *J Neurosci* 33, 11949-11959.
- S6. Chichilnisky, E.J. (2001). A simple white noise analysis of neuronal light responses. *Network* 12, 199-213.
- S7. Kerschensteiner, D., Liu, H., Cheng, C.W., Demas, J., Cheng, S.H., Hui, C.C., Chow, R.L., and Wong, R.O. (2008). Genetic control of circuit function: Vsx1 and Irx5 transcription factors regulate contrast adaptation in the mouse retina. *J Neurosci* 28, 2342-2352.